EFDA–JET–PR(10)72

M.I. Airila, D. Matveev, J.P. Coad, S. Brezinsek, M. Groth,
A. Kirschner, J. Likonen, M. Rubel, J.D. Strachan,
A.M. Widdowson, S. Wiesen and JET EFDA contributors

# Local Deposition of Injected $^{13}C$ Tracer at the Outer Divertor of JET

# Local Deposition of Injected $^{13}C$ Tracer at the Outer Divertor of JET

M.I. Airila[1], D. Matveev[2], J.P. Coad[3], S. Brezinsek[4], M. Groth[5], A. Kirschner[4], J. Likonen[1], M. Rubel[6], J.D. Strachan[7], A.M. Widdowson[3], S. Wiesen[4]
and JET EFDA contributors*

***JET-EFDA, Culham Science Centre, OX14 3DB, Abingdon, UK***

*[1]VTT Technical Research Centre of Finland, Association EURATOM-Tekes, P.O.Box 1000, FI-02044 VTT, Finland*
*[2]Department of Applied Physics, Ghent University, Plateaustraat 22, B-9000 Ghent, Belgium*
*[3]EURATOM-CCFE Fusion Association, Culham Science Centre, OX14 3DB, Abingdon, OXON, UK*
*[4]Institute of Energy and Climate Research – Plasma Physics, Forschungszentrum Jülich, Association, EURATOM-FZJ, Partner in the Trilateral Euregio Cluster, Jülich, Germany*
*[5]Aalto University, Association EURATOM-Tekes, P.O.Box 14100, FIN-00076 Aalto, Finland*
*[6]Alfvén Laboratory, Royal Institute of Technology (KTH), Association EURATOM-VR, SE-10044 Stockholm, Sweden*
*[7]Princeton Plasma Physics Laboratory, James Forrestal Campus, Princeton, NJ 08543, New Jersey, USA*
** See annex of F. Romanelli et al, "Overview of JET Results", (23rd IAEA Fusion Energy Conference, Daejon, Republic of Korea (2010)).*

Preprint of Paper to be submitted for publication in
Nuclear Fusion

**ABSTRACT**

The 2004 tracer experiment of JET with injection of $^{13}CH_4$ into H-mode plasma at the outer divertor has been modelled with the Monte Carlo impurity transport code ERO. EDGE2D/NIMBUS solutions for inter-ELM and ELM-peak phases were used as plasma backgrounds. Local 2D deposition patterns at the vertical outer divertor target plate were obtained for comparison with post-mortem surface analyses. ERO also provides emission profiles for comparison with radially resolved spectroscopic measurements. Modelling indicates that enhanced re-erosion of deposited carbon layers is essential in explaining the amount of local deposition. The measured local deposition of 20–34% is roughly reproduced if it is assumed that all returning hydrocarbons are reflected from the surface, the re-erosion of deposits is enhanced compared to graphite erosion and that ELMs contribute to the re-erosion. Modelled poloidal deposition profiles are very similar to the measured ones. The shape of deposition pattern is strongly affected by the divertor geometry near the injection point which casts a shadow onto neighbouring tiles. Deposition at the shadowed area and inside tile gaps was simulated separately with a simple model included in ERO and with the 3D Monte Carlo code 3D-GAPS. In gap simulations more than 10% of injected carbon is deposited in the gap and about 15% lost under the tiles, consistent with the picture obtained from post mortem analysis and EDGE2D/NIMBUS modelling.

## 1. INTRODUCTION

Tracer injection experiments in tokamaks provide information on material migration and deposition under constant plasma conditions. In plasma devices with carbon plasma-facing components a suitable tracer is the natural isotope $^{13}CH$ that can be distinguished from $^{13}CH_4$ in post-mortem surface analyses. The principal carbon migration can be investigated by injecting a tracer containing molecule such as CH from a net erosion zone, which is a strong impurity source also in the absence of injection. A molecular tracer substance imitates particularly well chemically eroded impurities. Carbon migration in plasma is a complex process starting from physical or chemical erosion of the surface by particle bombardment, followed by dissociation and ionization of molecules and atoms to ions and their transport under the influence of electromagnetic forces, plasma flow and diffusion. Finally, the eroded or injected particles are deposited on the plasma-facing surfaces, where re-erosion may occur, or on remote areas. The diagnostic capabilities for studying the details of this process are limited: the density distributions of impurity species in the plasma during the discharge can be obtained in situ by spectroscopic measurements of their light emission (see, e.g. [1]), and the final tracer distribution on plasma-facing components can be measured ex situ by e.g. ion beam techniques—for an overview, see [2]. Interpretation of these measurements for complete understanding of carbon migration requires in addition computer simulations.

The modelling of global migration of $^{13}CH$ in JET injection experiments is described in a comprehensive manner in [3]. The computational tool was the 2D fluid code EDGE2D supplemented with specially tailored post-processors to extend the modelling to re-erosion. EDGE2D uses the

Monte Carlo code NIMBUS, or alternatively EIRENE, to model neutrals. The present paper reports a more detailed modelling of the local effects at the divertor which are out of reach of EDGE2D. The main numerical tool in this work is 3D impurity transport code ERO [4,5] that has a more comprehensive physics basis for plasma–surface interaction processes, can describe the break-up chain of methane, and can cope with the toroidal inhomogeneity of the injection. In the global scale, modelling in 2D can be justified by tha fact that the injection was toroidally distributed although not completely uniform. The effect of molecular processes, instead, can be amplified by the fact that the injection was done rather close to the separatrix – therefore the SOL impurity source in the global model can be sensitive to the actual local dispersion of the tracer. Some initial modelling results that support the EDGE2D work were already reported in reference [3], and, conversely, the plasma solutions computed with EDGE2D are used as input for ERO in the present work. A less developed version of the reference with some parameter variations was already presented in reference [6]. For this work, the reference case was upgraded to include carbon impurities in the background plasma and the effect of neutral collisions on test particles. Moreover, the gap model, ELM modelling, spectroscopy analyses, investigation of particle loss distribution and more detailed description of the simulation method are novel material consituting the majority of the present contribution.

The geometry of the outer divertor implies a shadowed region around the injection location. The shadowing effect has been modelled with a simple model in the ERO code itself and—in parallel—with a more detailed gap deposition model 3D-GAPS [7,8] developed recently for evaluating the deposition in the tile gaps and castellated structures planned for ITER.

## 2. EXPERIMENT

On the final experimental day of JET campaign prior to installation of the HD divertor in 2004, 31 successful identical discharges (between Pulse No's: 63405–63445) were run with $^{13}CH_4$ injection from 48 injection modules (GIM 10) toroidally distributed around the outer divertor. The discharges were 1.4 T, 1.4 MA H-mode with line-averaged density of $2.9\times10^{19}m^{-3}$, 5MW NBI, 2.7MW ICRH and 120Hz 30kJ ELMs in hydrogen plasma. During $^{13}CH_4$ puff there was no additional fuelling and $Z_{eff}$ was about 2. The total injected amount was $4.3\times10^{23}$ particles. The magnetic configuration, ERO simulation volume and spectroscopy sight-lines are shown in figure 1. The gas injection module GIM 10 is located in the gap between tiles numbered poloidally as 7 and 8. Subsequent post mortem surface analysis delivered deposition profiles along various measurement lines, and the total amount of C deposited on Tiles 7 (see photo of Tile G7B in figure 2) and 8 has been estimated to $7.3\times10^{22}$ particles (17% of injection) [9]. Part of deposition is actually located on the horizontal part of Tile 8 but it is not found on all toroidal sections and therefore difficult to quantify globally. The relative locally deposited amount is denoted as "local deposition" or "net deposition", and in the modelling the simulation volume has been selected to match the measured area, making a direct comparison to experiment possible. In the course of simulation the gross deposition can be several times higher than net deposition, the majority of deposit being re-eroded as shown in section 4.1.

Tracer injection experiments avoid the complexities characteristic for long-term plasma–wall interaction studies in which various plasma configurations are involved over a period of months or years. However, some difficulties for modelling still arise from the uncertainties in the 2004 tracer injection experiment. It was found afterwards that part of the injected methane had been able to leak behind the divertor tiles and enter the vessel on top of the outer baffle, and possibly also in the Private Flux Region (PFR). The amount of leakage has been estimated in EDGE2D modelling [3] to be in the range 15–50 %. In modelling the full injection rate was used, but the leakage has been taken into account when comparing modelling results to post mortem analyses by scaling up the measured deposition of 17 % to 20–34 %.

Relevant diagnostics in the present experiment include spectroscopy and surface analyses. The KT3 spectrometer provides 12 radially separated, line integrated signals in front of the outer divertor target. Emission lines CII at 426.7 nm, CII at 514.0 nm and CI at 909.5 nm and the CH A-X band at 431.0 nm were acquired prior to and during the puff. Post mortem measurements of Tile 7 cover the shadowed surface facing the plasma (see figure 3), several measurements with Enhanced Proton Scattering (EPS) with 2.5MeV H ions along toroidal lines, and Secondary Ion Mass Spectrometry (SIMS) measurements along two poloidal lines. 3D-GAPS modelling results can be compared to the measurements in the shadow and the actual ERO deposition pattern to the measurements on the plasma-facing surfaces.

## 3 SIMULATION METHOD

### *3.1 THE ERO CODE*

ERO is a 3D Monte Carlo impurity transport code for modelling the motion of impurity particles in plasma [e.g. tokamak Scrape-Off Layer (SOL) or linear plasma simulator]. It accounts for atomic physics and relevant chemistry through external databases. For advanced plasma–surface interaction modelling ERO has been coupled to the SDTrimSP code (based on the binary collision approximation valid at impact energies above ≈50eV) [10,11]. The present simulations use the Homogeneous Material Mixing surface model (ERO-HMM), which provides sufficient accuracy in the case of carbon injection on a carbon surface and is faster than SDTrimSP. ERO-HMM assumes that different atomic species are homogeneously mixed in a surface layer of certain thickness (approximately the ion range in the solid surface material). The erosion yield of each species from a surface cell is read from the database and the resulting erosion rate is proportional to the concentration in the interaction layer of the cell.

The simulations proceed in discrete time steps during which the surface composition is kept constant. Within each (surface) time step a much shorter (particle) time step is used for particle tracing, which can be further decreased in the vicinity of the surface. The surface time step is limited by the requirement that one must not erode more particles than there are in the interaction layer of a surface cell. The erosion rate reaches its maximum at the strike point, and erosion is highest for deposited amorphous carbon layers (assumed enhanced erosion yield of 20%). The resulting

erosion rate at the divertor can be properly handled by the surface model if the surface time step is 0.005 seconds. For ELM modelling a shorter surface time step of 0.1ms was used for the ELM peak, as explained in detail in section 4.3. The simulation volume shown in figure 1 extends 750 mm toroidally, encompassing two injector locations 560mm apart. A periodic boundary condition was applied for the test particles in the toroidal direction to simulate the effect of 48 injectors located around the torus. The poloidal extent is 160 mm (30 mm into the Private-Flux Region (PFR) and 130 mm into the SOL at target). Also the radial dimension of the volume is 160mm.

### *3.2 REFERENCE CASE FOR MODELLING*

In the modelling a "reference case" was selected as a starting point and parameter variations were carried out in order to evaluate the significance of different assumptions and to find out whether the match to measurements could be improved. The reference case is defined by the following input parameters: The effective sticking coefficient of hydrocarbons S is assumed to be zero, describing either reflection or prompt re-erosion of deposited particles. Reflection of atoms and ions is calculated from TRIM data. The chemical erosion yield is fixed to 2% for the substrate, but physical and chemical re-erosion of deposited material is enhanced by a factor of 10 (see references [12-14]; the effect of this number was studied with parameter variations). The temperature and flux dependences of chemical erosion have been neglected. Particle reflection, sputtering by test particles and the background plasma, perpendicular diffusion and thermal force are included in the simulation. The total injected amount of $4.3\times10^{23}$ molecules of $^{13}CH_4$ in the experiment was assumed to be distributed over 200s of plasma time and evenly over the 48 injectors, giving an injection rate of $4.47\times10^{19}$ particles/s for each source point. The plasma background is the inter-ELM EDGE2D solution with 4% carbon content assumed in ERO. In addition the neutral gas density was set to $10^{20}$ $m^{-3}$. The external source is represented by 10 000 test particles and the eroded flux by 4800 test particles on each time step, giving good statistics for individual surface cells in most of the SOL. In the PFR (where deposition is toroidally uniform) the deposition was averaged toroidally to increase the sample size. Regarding Monte Carlo noise, a standard deviation below 20% is obtained except at the poloidal positions of about –25mm and +20mm (see figures in section 4.1). In the time traces of net deposition there are fluctuations of about 1.5 percentage units between time steps, but the fitting procedure provides the steady-state deposition with an uncertainty of about 0.2 percentage units. Tracing of the test particles in the plasma takes most of the computing time, totalling 1–3 hours per time step on a single core of a quad-core processor. About 60 iterations were needed for convergence in the reference case.

### *3.3 MODEL FOR THE GAP AND SHADOWED REGION*

Tile 8 shadows the top edge of Tile 7 from plasma so that the injected methane can possibly form a gas pocket in front of the injection location and erosion/deposition balance is different from that on plasma-wetted surfaces (see figure 17 of reference [3]). The dimensions of the shadowed region

are a few millimetres. Significant, toroidally symmetric deposition has been found at the upper part of Tile 7 [15]. This deposition was first interpreted to be located in the shadowed surface of the tile, but the poloidal dimension of the shadow is so small that the highest deposition is in fact on a plasma-intersecting surface. Moreover, the measurements show that the horizontal surface of Tile 7 and the adjacent narrow shadowed stripe are practically clean. The present modelling work was carried out with the interpretation that the shadow is the main deposition zone, which led to the development of the shadow model (suppression of re-erosion where highest deposition is found). Although the agreement to measurements is good, the interpretation should be different. A possible explanation would be that the injected gas has locally detached the plasma in front of the injection point so that a similar reduction in the re-erosion rate has occurred as in the model.

To explain the low deposition in the gap and shadow the 3D-GAPS code is required for a proper treatment of the geometry. The simulations were refined in steps, applying two models with different level of detail:

- The first modelling approach was to assume that the tiles form a planar surface and apply a modified plasma background in ERO. Re-erosion is prevented on a surface region representing the shadow by setting the plasma temperature and density to almost zero within a few millimetres from the surface. However, this approach neglects the existence of the gap altogether and any geometry effects that affect the velocity distribution of plasma particles and neutrals. On the other hand, effects of parameter variations can be studied since the simulations can be run with reasonable manual effort.
- To model the deposition also inside the tile gap, ERO and 3D-GAPS were combined as shown in figure 4. In the present work the interchange of data between ERO and 3D-GAPS was performed manually, but ongoing efforts aim at a direct coupling of the two codes for integrated modelling of gap deposition and impurity transport. To a first reasonable approximation a three-step calculation is needed:
  (i) (Iteration 0) The transport of $CH_4$ from the gas injection module to plasma is calculated with 3D-GAPS, using $10^6$ test particles per injector. The same injection rate and injection locations are used as in ERO, but the particles start from the bottom of the gap as $^{13}CH_4$ with an isotropic velocity distribution and cosine reflection with $R_N = 1$ assumed.
  (ii) (Iteration 1) The resulting spatial and velocity distribution of particles is used as the source in ERO (instead of the point source used in the reference case simulation). The simulation time of 0.5s is divided into 100 time steps. ERO accounts for erosion of tiles by plasma ($D^+$) and impurity ($C^{x+}$) ions, break-up of hydrocarbons and ionization. Particles returning into the gap are recorded.
  (iii) (Iteration 2) Particles returning to the gap are simulated again with 3D-GAPS. As they may now stick to the surfaces, the resulting surface distribution is recorded. ERO provides two distinct sources of particles: injection and erosion. Sputtering, chemical erosion, and elastic collisions are taken into account.

The results obtained with this model are reported in section 4.2.

### *3.4 THE 3D-GAPS CODE*

Similar to ERO, the Monte-Carlo neutral transport code 3D-GAPS [8] uses the test particle approach to describe the 3D transport of impurity atoms in a gap. Test particles originate either directly from plasma (e.g., can be provided from ERO simulations) or as recycled or eroded neutrals and radicals from plasma-wetted or remote surfaces. As plasma penetration into the gap is weak, the emphasis is put on transport of neutrals traveling along straight paths until they reach any surface or undergo an elastic collision. Plasma penetration into the gap can also be taken into account via coupling with a Particle-In-Cell (PIC) model [16]. Being a powerful method for sufficiently narrow gaps and certain range of plasma parameters, PIC simulations could not be applied in the present set-up as the gap is so wide (12mm) compared to the Debye length that simulations would become excessively time-expensive.

## 4. SIMULATION RESULTS

### *4.1 REFERENCE CASE*

Figure 5 shows the temporal evolution of deposition efficiency towards equilibrium in the reference case. Starting from a clean carbon surface, injected C starts building up layers mainly downstream of the injection points. At the beginning of the simulation there is not yet any re-erosion and a deposition efficiency of about 80 % is found. This illustrates only how efficiently the plasma returns injected particles onto the surface and how prone they are to stick. The remaining about 20 % escapes into the PFR and SOL. As the layer builds up, re-erosion starts releasing some of the deposited carbon and the loss rate increases. After about 0.3 seconds of simulation time (time scaling is dependent on the selected interaction layer thickness) an equilibrium surface concentration distribution is reached and the net deposition rate levels off at about 40 % of the injection rate. This number is representative for experimental comparison, since the plasma durations are much longer than the initial transient mentioned above. In the steady state, the dominant escape route is into the PFR, some carbon still ending up into the SOL.

Apart form the coupled ERO/3D-GAPS simulations, the most complete model in the present work is the reference case supplemented with ELM modelling. It turns out that this case also reaches the best agreement to measured deposition – therefore figures 6 and 7 show the 2D deposition pattern and deposition profiles along lines used in post mortem analyses, respectively, after ELMs have been applied to the reference case (see section 4.3 for a complete description of the ELM simulation technique). One can clearly see that the plasma flow along **B** drags the carbon downstream and that it is mostly deposited within some tens of centimetres from the source. The tail from the injector on the right reaches the "SIMS B" measurement line and produces a clear footprint there. The toroidally extending deposition stripe between injectors represents the accumulation of $^{13}C$ in the area shielded from direct bombardment of plasma ions. Finally, the role of neutral collisions is strong in dispersing the injected carbon towards PFR in a way that produces significant deposition at the poloidal location of about –100mm. At the outer strike point area, however, re-erosion is so

strong that a minimum appears in the accumulated carbon profile. In the poloidal profiles – both measured and modelled – one can easily see three different maxima resulting from these migration processes.

Comparing the spectroscopy output of ERO to measurements is not straightforward since the KT3 spectrometer sees a strong contribution from the radiation at the separatrix. To imitate this effect in ERO, one needs to add test particles ending up homogeneously to the separatrix. This can be done by imposing an additional CH flux from the PFR. Combining this "intrinsic" emission to the "extrinsic" emission from the injection it is found that the PFR methane flux should be 25 times higher than the puff for best match between the measured and simulated profiles. However, ERO cannot account for the increase of the background impurity content arising from the injected particles circulating through the main plasma. These impurities increase the emission almost homogeneously (figure 8) while the test particles in ERO have a much more localised effect on emission profiles (figure 9).

### *4.2 DEPOSITION IN THE GAP AND LOSSES BEHIND TILES*

For 3D-GAPS modelling, the realistic geometry of the gap between Tiles 7 and 8 was implemented as shown in figure 4. The gap width is 12mm, toroidal length 750 mm and depth 23mm (plasma open side) / 32.2mm (plasma shadowed side). Local magnetic field direction defines the interface to the ERO simulation volume. The assumptions made in the 3D-GAPS model are:

- Fixed reflection coefficient (cosine) for each type of species (also for $CH_x$): $R(c) = 5\times10^{-4}$, R ($CD_1$) = 0, R ($CD_2$) = 0975, R ($CD_3$) = 0.999 and R ($CD_4$) = 1 (also as a product of chemical erosion)
- No energy/angular dependence of the reflection coefficient
- No energy loss (reflection with the same energy)
- Isotropic elastic collisions only with one type of species, e.g. D or $D_2$
- Chemical erosion by D atoms is due to a uniform isotropic flux into the gap
- Particles landing outside geometrical shadow considered as lost
- Particles crossing the gap bottom considered as lost under the tiles

The resulting deposition rate profile over the gap perimeter (toroidally averaged) is shown in figure 10. More than 10% of the injected carbon is deposited and about 15 % lost under the tiles.

There are considerable uncertainties concerning the neutral deuterium density in the vicinity of the gap and the resulting D flux onto gap walls. Increasing neutral density restricts the motion of test particles in the gap and leads to increasing trapping of C inside the gap. On the other hand, neutral flux onto the surfaces affects the deposition efficiency through chemical erosion (assumed $Y_{chem}$ = 2%). Although neutral density and flux are partly correlated, they were varied separately over a wide range (flux $\Gamma(D^+)$ $10^{16}$... $10^{21}$ $cm^{-2}$ $s^{-1}$, density n = $10^{12}$... $10^{15}$ $cm^{-3}$). It can be concluded that neutral collisions do not have significant effect, unless the neutral density is unrealistically high (well above $10^{14}$ $cm^{-3}$). Chemical erosion for the $D^0$ flux of $5\times10^{18}$ $cm^{-2}$ $s^{-1}$ and above, in

turn, affects the results by decreasing the deposition and leading to higher losses of particles under the tiles.

### 4.3 ELMS

As a result of the investigations of global migration [3] there are EDGE2D plasma backgrounds available both for the inter-ELM phase and for the ELM peak. The major difference between these is in temperatures. The inter-ELM plasma has $T_e \approx T_i < 5$eV at the target while during ELMs target $T_e$ reaches 130eV and $T_i$ exceeds 200eV. In the present work these plasma solutions were used to perform a simple study of the effect of ELMs on local migration. Once the reference case reached its equilibrium surface composition (with the inter-ELM plasma background), successive time steps with alternating ELM-peak and inter-ELM plasma backgrounds were simulated for 126 ELM cycles (0.64s). The lengths of the time steps were chosen to be 0.1ms for the ELM peak and 5ms for the inter-ELM phase, matching roughly the real durations of these phases. ELM dynamics is not completely described by this method, e.g. the strike point movements are neglected.

The time evolution of net deposition between ELMs and net erosion during ELMs is shown in figure 11. Adding these numbers one can obtain the net deposition over the whole ELM cycle. At the onset of ELMs the net deposition drops from the equilibrium value of 40% to about 31% but raises quickly (in about 0.3s) back to about 37 %. Within individual cycles there is net erosion during ELM-peak (almost 10% of injection over the whole cycle) and net deposition between ELMs (at the beginning 40%, then saturation at 45%). Obviously the ELMs repeatedly deplete the deposition zone from $^{13}C$, reducing its concentration in the interaction layer and thus erosion rate, which allows a higher inter-ELM net deposition rate to be sustained than in the case of a constant plasma background. Increased erosion during ELMs is due to a higher temperature and somewhat higher particle flux, which increases the physical sputtering rate to a level sufficient to cause significant erosion during the short peak-ELM phase. This way ELMs lead to some redistribution of deposited carbon, and after a short transient a new equilibrium surface distribution is obtained. Because of small ELM size (30kJ), thermal decomposition of deposited layers should not have any significant contribution to erosion [17].

The distribution modelled this way reproduces almost perfectly the SIMS measurements – both the locally deposited fraction estimated to 20–34% in the experiment and the poloidal profiles as shown in figure 7. This match is closer than one would expect in view of the uncertainties related to modelling assumptions and data as well as the fact that and the simulation parameters were not particularly tailored to achieve best agreement. In fact the uncertainties were handled by carrying out an extensive set of parameter variations around the reference case as described in reference [6]. The results of these parameter variations are briefly summarized in table 1. In addition to the results shown in the table, the re-erosion enhancement factor $f_{re}$ was varied between 1 and 10 with the obvious result that the locally deposited fraction becomes significantly larger than measured if the factor is below 10. This result is an update for reference [6], where the simulations lacked

carbon impurity in the plasma background and the effect of neutral collisions. This led to the early conclusion that $f_{re}$ should lie in the range 2.5…7 to reproduce the measured local deposition. Neutral collisions also enhance significantly the migration of carbon into the PFR, which allows reproducing the measured deposition further away from the injection location.

## SUMMARY AND DISCUSSION

Local deposition modelling for the 2004 JET divertor tracer injection experiment was carried out with the ERO code using EDGE2D plasma backgrounds. Measured $^{13}C$ distributions can be closely reproduced by assuming negligible effective sticking of hydrocarbons, enhanced re-erosion of deposits, no re-erosion in the shadowed areas, and including ELMs in the simulation with a simple model. The effect of ELMs is addressed by using different fluid plasma solutions as the plasma background in ERO. The simulated emission from carbon species was compared to spectroscopy by assuming an intrinsic carbon flux to separatrix in addition to the injection. The emission profiles can be made somewhat similar only by assuming that the intrinsic flux is 25 times more intense than the injection. Sensitivity of the results was studied with parameter variations, indicating that under the prevailing uncertainties the achieved consistency between simulations and measurements is actually better than one should expect. For instance, electric fields and related drifts have been shown to be significant for impurity migration in the divertor region [18,19], but they were neglected in the present work due to the lacking capability of EDGE2D to model impurities and drift simultaneously.

The results rely on the assumption that there is a region of low re-erosion immediately next to the injection location. This model was designed to describe the shadowing effect of Tile 8 in the light of an early interpretation of post-mortem analysis results. The extensive analysis with the ERO code was already completed before the revision of the interpretation (the shadow is much smaller, just a few millimetres poloidally). Close match to the measured profiles leads one to seek an alternative explanation for reduced re-erosion on this area. One candidate could be local detachment of the plasma due to the tracer injection. So far it has not been estimated whether the $^{13}C$ influx would be capable of producing locally such an effect.

Independently of the shadow model, $^{13}C$ deposition in the gap and possible penetration behind the tiles were studied using the 3D-GAPS code. Modelling with a chemical erosion yield of 2% and simplifying assumptions on particle reflection suggests that more than 10 % of injected carbon could be deposited in the gap and about 15% of injected particles could be lost under the tiles (e.g. pumped out or find a leakage route into the main chamber). This is in line with the estimate of 15–50% leakage obtained from EDGE2D modelling. However, recalling that molecules are not allowed to escape through the gap bottom during iteration 0 and that the simulation ends after iteration 2, the above given numbers represent just a lower limit. The deposition/trapping efficiency should increase if direct leakage of injected molecules under the tiles (into plasma or pumping ducts) and iterative return of particles into the gap were accounted for. It can be estimated, for instance, that only the iterative return of particles into the gap will lead to an increase of the overall trapping efficiency

(deposition in the gap plus loss under the tiles) from about 25% to almost 40% in the standard case. Assuming 25% direct leakage of injected molecules during iteration 0, this value will rise further to above 50%.

The rapid fall-off of the deposition in the shadow (figure 10) is consistent with the experimental observation that the shadow and top surface of Tile 7 are practically clean. At the very edge of the shadowed region 3D-GAPS predicts rather high deposition density which can be attributed to ions still penetrating into this region. Although such a deposition density is several times larger than the highest measured density, this extremely narrow region was not included in the measured samples available. Moreover, the results in this critical area on the border of ERO and 3D-GAPS simulation domains are very sensitive to erosion assumptions and could not be taken as a reference. In the near-by region completely shadowed from ions, the deposition density is in good agreement with the measurements.

Elastic collisions for the residual neutral densities up to $10^{15}$ $cm^{-3}$ were found to be either negligible or having very weak effect for the deposition in the gap. Chemical erosion under neutral deuterium fluxes up to $5\times10^{18}$ $cm^{-2}s^{-1}$ was found to have rather small effect on the integral trapping efficiency. Higher deuterium fluxes ($10^{18}$ $cm^{-2}s^{-1}$ and above) were found to decrease significantly the deposition rate in the gap itself while increasing the loss rate under the tiles finally leading to lower integral trapping efficiency (deposition + loss). Under experimental conditions chemical erosion should not have significant influence.

After the injection analysed here, JET has continued its series of local injection experiments supplemented with ERO modelling, in 2007 with $^{12}CD_4$ [20,21] and in 2009 with $^{13}CH_4$ [22]. Related modelling is ongoing and will provide further insight into deposition/re-erosion behaviour in divertor plasmas, facilitating the extrapolation of tritium retention to ITER.

## ACKNOWLEDGEMENTS

This work was supported by EURATOM and carried out within the framework of the European Fusion Development Agreement. The views and opinions expressed herein do not necessarily reflect those of the European Commission. The work was partially funded by the Academy of Finland project No. 134930. Computing resources have been provided by CSC, the Finnish IT Centre for Science. CSC is owned by the Ministry of Education.

## REFERENCES

[1] Brezinsek S 2007 Journal Nuclear Materials **363–365** 1119
[2] Rubel M, Coad J.P, Hole D and JET-EFDA Contributors 2005 Vacuum **78** 255
[3] Strachan J.D. 2008 Nuclear Fusion **48** 105002
[4] Naujoks D, Behrisch R, Coad J.P. and De Kock L.C.J.M. 1993 Nuclear Fusion **33** 581
[5] Kirschner A, Philipps V, Winter J and Kögler U 2000 Nuclear Fusion **40** 989
[6] Airila M I 2009 Physica Scripta **T138** 014021

[7] Matveev D 2008 Modelling of material deposition in the gaps of castellated surfaces in fusion experiments Master thesis (Ghent University)
[8] Matveev D, Kirschner A, Litnovsky A, Komm M, Borodin D, Philipps V and Van Oost G 2010 Plasma Physics and Controlled Fusion **52** 075007
[9] Coad J.P. 2007 Journal Nuclear Materials **363–365** 287
[10] Eckstein W, Dohmen R, Mutzke A and Schneider R 2007 SDTrimSP: A Monte Carlo code for calculating collision phenomena in randomized targets IPP Report 12/3 (Max-Planck-Institut für Plasmaphysik)
[11] Droste S, Kirschner A, Borodin D, Kreter A, Brezinsek S, Philipps V, Samm U, Schmitz O and the TEXTOR team 2008 Plasma Physics and Controlled Fusion **50** 015006
[12] Wienhold P, Esser H.G, Hildebrandt D, Kirschner A, Mayer M, Philipps V and Rubel M 2001 Journal Nuclear Materials **290–293** 362
[13] Kirschner A, Brooks J.N, Philipps V, Coad J.P. and contributors to the EFDA-JET Workprogramme 2003 Plasma Physics and Controlled Fusion **45** 309
[14] Kirschner A, Wienhold P, Philipps V, Coad J P, Huber A, Samm U and JET EFDA contributors 2004 Journal Nuclear Materials **328** 62
[15] Coad J P 2008 Local deposition of the C tracer at the JET MkII-SRP outer divertor 9th Int. Workshop on Hydrogen Isotopes in Fusion Reactor Materials (Salamanca)
[16] Dejarnac R and Gunn G.P. 2007 Journal Nuclear Materials **363–365** 560
[17] Kreter A, Esser H.G, Brezinsek S, Coad J.P, Kirschner A, Fundamenski W, Philipps V, Pitts R.A. and Widdowson A. 2009 Physical Review Letters **102** 045007
[18] Aho-Mantila L. 2010 Journal Nuclear Materials (in press) doi:10.1016/j.jnucmat.2010.10.080
[19] Aho-Mantila L. 2011 Influence of magnetic field reversal on the divertor plasma and its impact on local carbon migration in ASDEX Upgrade Nucl. Fusion (submitted)
[20] Brezinsek S. 2009Journal Nuclear Materials **390–391** 267
[21] Airila M.I. 2010 Journal Nuclear Materials (in press) doi:10.1016/j.jnucmat.2010.11.054
[22] Likonen J. 2011 Deposition of C tracer in the JET MKII-HD divertor 13th Int. Workshop on Plasma-Facing Materials and Components for Fusion Applications (Rosenheim)

| Simulation case | Deposited | Loss $x_{min}$ | Loss $z_{max}$ | Loss $x_{max}$ |
|---|---|---|---|---|
| Reference | 40% | 16% | 28% | 16% |
| With ELMs | 36% | 16% | 28% | 20% |
| No shadow | 38% | 17% | 29% | 16% |
| No shadow, S = 0 .7 | 77% | 5% | 10% | 8% |
| No thermal force | 62% | 13% | 0% | 25% |
| S = 0 .7 | 78% | 4% | 10% | 8% |
| $C^0$ injection at 0.05 eV | 79% | 5% | 12% | 4% |
| $C^0$ injection at 0.5 eV | 70% | 7% | 16% | 7% |

*Table 1: Net deposited fraction and the losses to various directions in equilibrium. The particles lost into the and directions enter the PFR, while the particles lost into the direction mainly enter the SOL.*

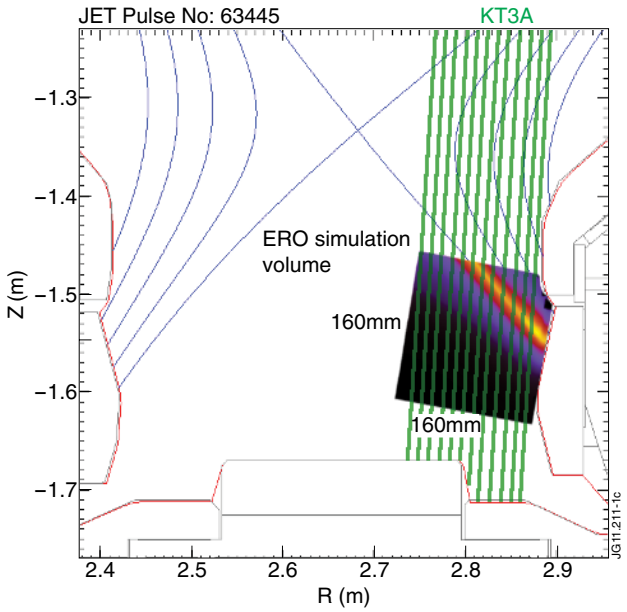


*Figure 1: Magnetic configuration and the simulation volume of ERO, with electron density from EDGE2D model. The sight-lines of KT3 visible spectrometer are plotted in green.*

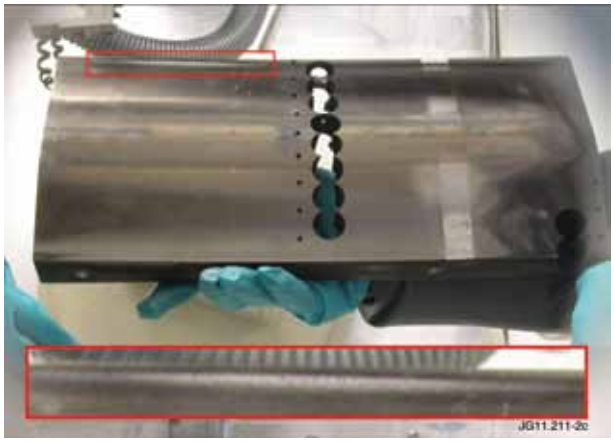


*Figure 2. Photo of $^{13}C$ distribution in the vicinity of puffing locations, Tile G7b. The inset shows the area of highest surface density of $^{13}C$, visible as a light gray cigar-shaped deposit at the very edge of the tile.*

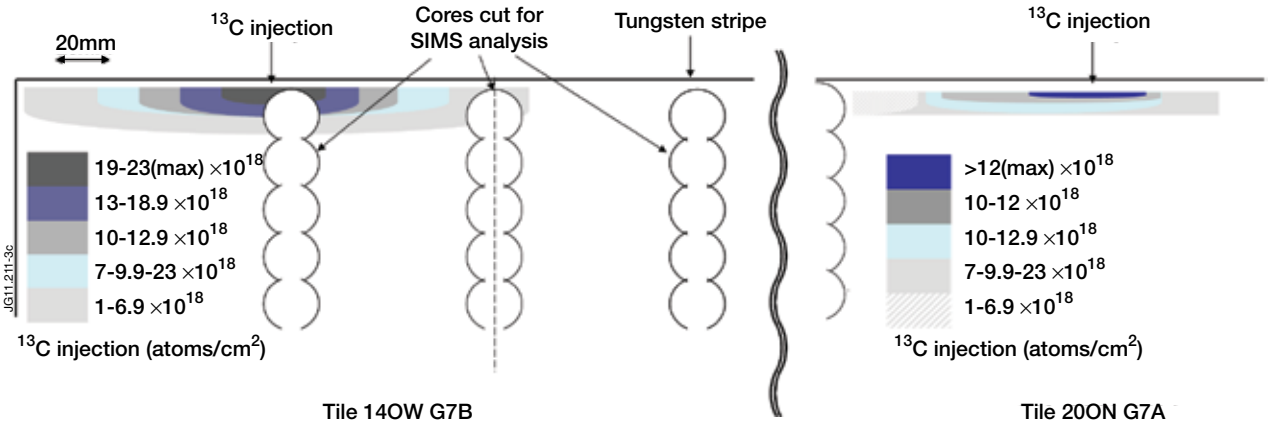


*Figure 3: Measured $^{13}C$ distribution in the vicinity of puffing locations, plotted schematically.*

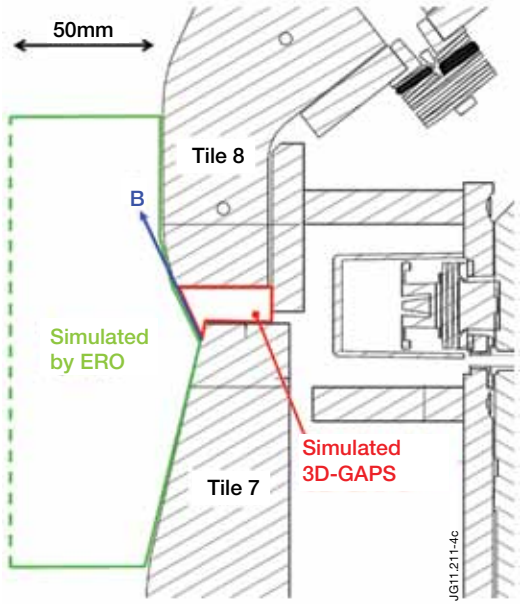


*Figure 4: Relation of the simulation volumes for ERO and 3D-GAPS on the outer divertor. The interface is defined by the magnetic flux surface just touching the corner of Tile 8.*

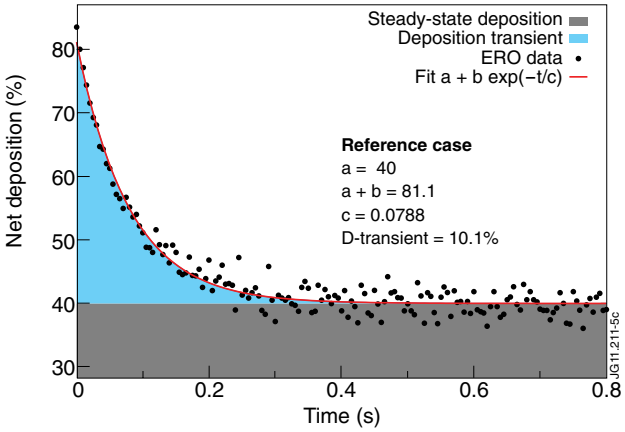


*Figure 5: Time evolution of net deposited fraction (relative to the injection rate and integrated over the whole simulated surface) in the reference case. The initial transient deposition (blue area) increases the simulated tracer accumulation shown in figure 7. After 0.8s (end of simulation) the excess amount is 10% of the deposition obtained at the steady-state rate over the same time interval (grey). Because the homogeneous material mixing surface model is used, the actual time scaling may not be realistic but depends on the selected interaction layer thickness, which is 5nm here.*

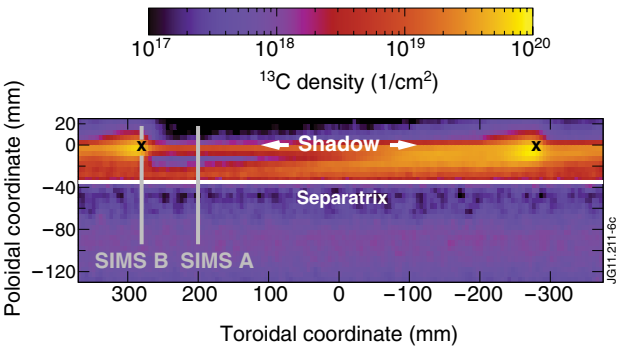


*Figure 6: Deposition pattern in the reference simulation after ELMs have been applied. Injector locations are marked with "x", the shadow extends toroidally across them and SIMS measurement lines are shown in grey.*

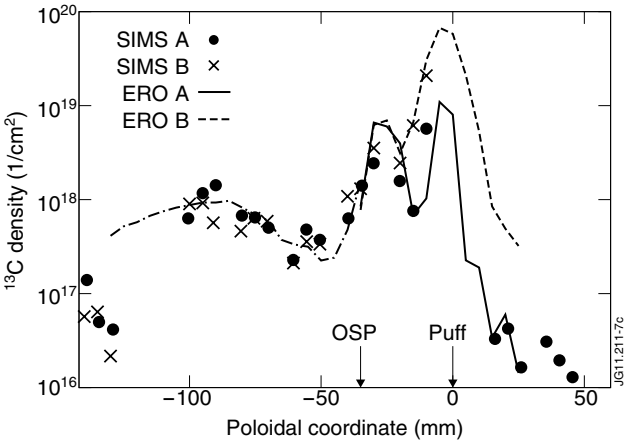


*Figure 7: Poloidal profiles of the deposition along SIMS measurement lines in the reference case after ELMs have been applied. Each of the samples (holes in figure 2 has been analysed at 3 locations. Lines: ERO simulation, markers: SIMS measurements along the lines shown in figure 2 of reference [6]. Left from the OSP the profile has been toroidally averaged to reduce noise.*

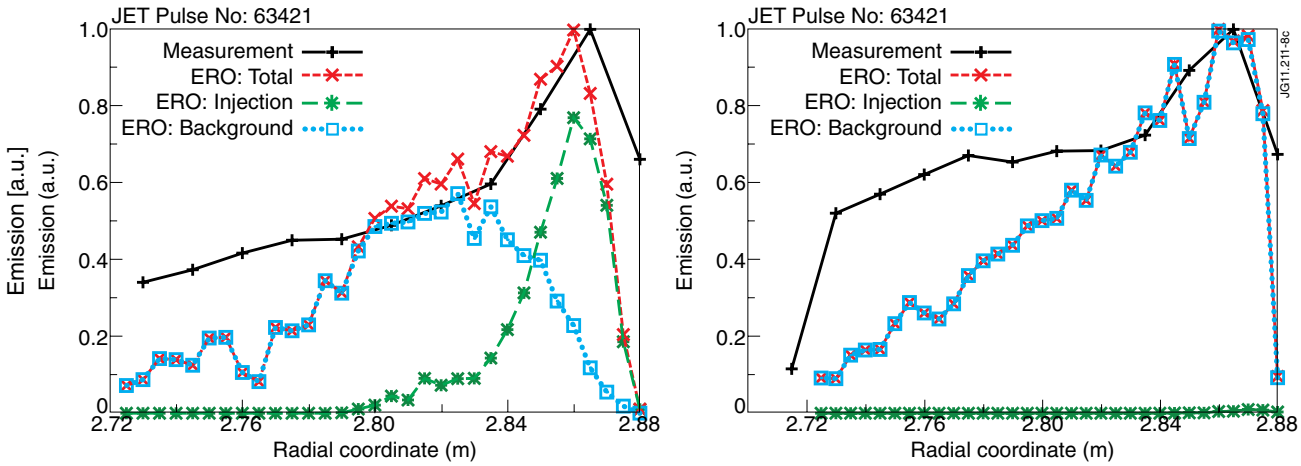


*Figure 8: Left: Emission profile of C II light as measured by the KT3 spectrometer before and during the puff. Right: Emission profile of CH light.*

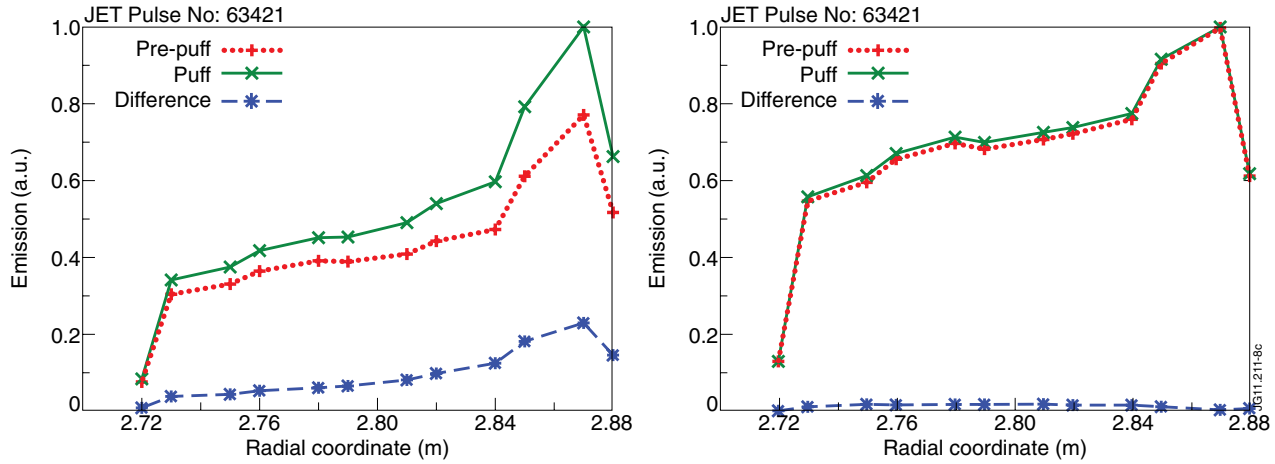


*Figure 9: Left: Emission profile of C II light as measured by the KT3 spectrometer. In the ERO model it has been assumed that a background $CH_4$ flux from the PFR 25 times higher than the injection is present (best fit). Right: Emission profile of CH light under the same assumption.*

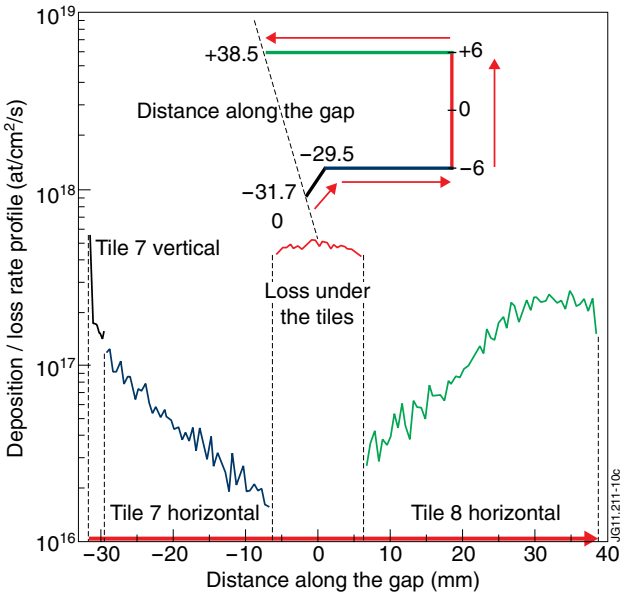


*Figure 10: Deposition rate profile of 13C on gap sides and loss under the tiles as simulated by 3D-GAPS. Inset: Definition of the coordinate along gap walls.*

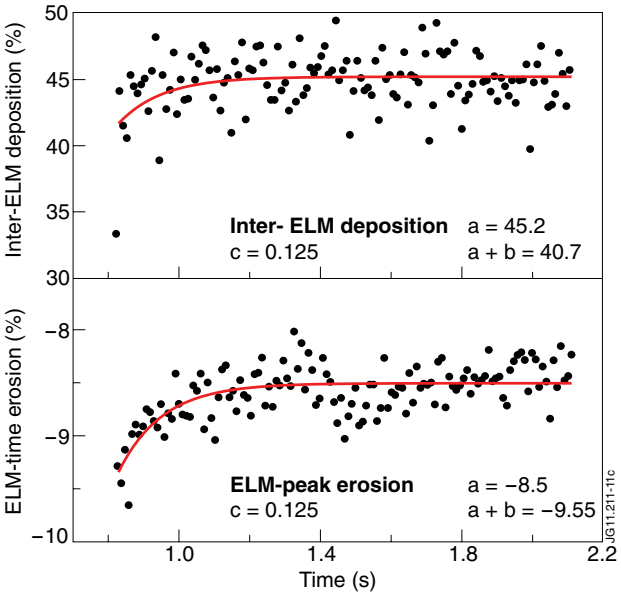


*Figure 11: Time evolutions of net deposition between ELMs (top) and net erosion during ELMs (bottom). The erosion/deposition is given relative to the injection during the ELM cycle. The data are fitted with $a + b\ \exp(-t/c)$ by using for inter-ELM deposition the value of c obtained from the erosion fit.*